Mathematics

https://www.aimspress.com/journal/Math

AIMS Mathematics, 11(8): 26677–26698.
DOI: 10.3934/math.20261070
Received: 26 June 2026
Revised: 26 July 2026
Accepted: 29 July 2026
Published: 25 August 2026

Research article

Integrability criteria and multi-wave solutions of a generalized variable-coefficient nonlinear evolution equation

Majid Madadi[1,2], Yakup Yildirim[3,4], Lanre Akinyemi[5] and Solomon Manukure[6,*]

[1] Department of Mathematics, Saveetha School of Engineering, Saveetha Institute of Medical and Technical Sciences, Saveetha University, Chennai 602105, Tamil Nadu, India
[2] Research Center of Applied Mathematics, Khazar University, Baku, Azerbaijan
[3] Department of Computer Engineering, Biruni University, Istanbul 34010, Turkey
[4] Mathematics Research Center, Near East University, 99138 Nicosia, Cyprus
[5] Department of Mathematics, Prairie View A&M University, Texas, USA
[6] Department of Mathematics, Florida A&M University, Tallahassee, FL 32307, USA

* **Correspondence:** Email: solomon.manukure@famu.edu.

Abstract: In this paper, we studied a (2 + 1)-dimensional variable-coefficient nonlinear evolution equation that generalizes several well-known models, including the Kadomtsev–Petviashvili, generalized second-order Benjamin–Ono, and Boussinesq equations. The integrability of the equation was investigated using Painlevé analysis, leading to explicit conditions on the variable coefficients. These conditions were shown to be consistent with the existence of multi-soliton solutions. By applying Hirota's bilinear method, we explicitly derived and verified one-, two-, three-, and four-soliton solutions. Their pairwise interaction structure motivates a proposed general N-soliton form. In addition, breather waves, lump solutions, and hybrid lump–soliton interactions were derived using appropriate ansatz methods. The effects of variable coefficients on wave behavior were illustrated through different solution structures. The results showed that variable coefficients play an important role in shaping wave dynamics and interaction patterns. This work extends existing results on nonlinear evolution equations and provides useful insight into wave propagation in inhomogeneous media.

Keywords: variable-coefficient equation; Painlevé analysis; soliton; breather wave; lump wave
Mathematics Subject Classification: 35C07, 35C08, 35Q53, 37K40

1. Introduction

Nonlinear evolution equations (NLEEs) play a central role in modeling complex dynamical systems where nonlinear effects and dispersion interact intricately. These equations emerge in a variety of scientific and engineering domains, including plasma physics [1], fluid dynamics [2], quantum mechanics [3], nonlinear optics [4], and many more [5, 6]. Understanding exact solutions of NLEEs is essential for describing physical phenomena and for predicting the behavior of both natural and engineered systems. A wide array of mathematical methods has been developed to study NLEEs and construct their exact solutions. The Darboux transformation [7] provides a systematic approach for generating new solutions from known ones, particularly for integrable systems. Bäcklund transformations [8] establish relations between different solutions and are useful for obtaining nonlinear wave structures. The inverse scattering transform [9] offers a powerful framework for solving integrable equations by connecting them with linear spectral problems. The sine-Gordon approach [10] and traveling-wave reduction [11] transform NLEEs into simpler forms, enabling the derivation of solitary wave solutions. Expansion methods, such as the $(\frac{G'}{G})$- and $(\frac{1}{G})$-expansion techniques [12–14], provide direct algebraic procedures for constructing exact solutions, while recent data-driven approaches, including neural networks [15, 16] and generative adversarial networks [17], offer alternative strategies for approximating and discovering nonlinear wave solutions. The M-fractional derivative method [18] has also been applied to investigate nonlinear models involving fractional effects.

Among these techniques, the Hirota bilinear method [19–21] stands out due to its flexibility in analyzing both integrable and non-integrable systems. By transforming nonlinear equations into bilinear forms, it provides a systematic framework for constructing various exact solutions, including multi-soliton, breather, lump, and hybrid wave structures. Moreover, it effectively describes nonlinear wave interactions, such as elastic collisions and energy localization. Owing to these advantages, the Hirota bilinear method has become a powerful tool for studying NLEEs, including variable-coefficient, higher-dimensional, and generalized dispersive systems. The fundamental solutions of NLEEs often involve nonlinear localized waves, such as solitons, breathers, and lumps. In integrable models, solitons are localized waves characterized by shape-preserving propagation and particle-like interactions. Their robustness has made them relevant in diverse fields, including nonlinear optics [22], oceanography [23], and plasma physics [24]. Breathers, in contrast, are nonlinear waves with energy concentrated in a localized, oscillatory pattern [25], while lump waves [26] represent high-energy solitary structures that can propagate as intense localized pulses. In oceanic contexts, lump waves are particularly important for predicting potentially destructive phenomena. Investigating the integrability properties of NLEEs is important for identifying equations that may support systematic families of exact solutions and rich nonlinear wave structures. Tools such as Painlevé analysis allow one to assess whether an equation can be consistently solved. Techniques including Ablowitz-Ramani-Segur (ARS) [27], Weiss-Tabor-Carnevale (WTC) [28], and Kruskal's simplification [29] facilitate checking the Painlevé property, which is closely tied to the existence of exact solutions. Moreover, the presence of N-soliton solutions typically signals integrability, as solitons are hallmark features of integrable systems.

Recently, variable-coefficient NLEEs have attracted significant interest because they model inhomogeneous media and systems with varying boundary conditions more accurately than constant-coefficient equations [30–32]. In many realistic physical environments, the properties of the medium are not uniform and may vary spatially or temporally due to changes in material parameters, external forces, geometrical effects, or environmental conditions. Consequently, variable coefficients provide a more realistic description of wave propagation in non-uniform media, where dispersion, nonlinearity, and coupling effects may evolve along the propagation direction. Such models have been widely employed to describe complex phenomena in fluid mechanics, plasma physics, nonlinear optics, and other areas where spatial inhomogeneity plays a crucial role. Compared with their constant-coefficient counterparts, variable-coefficient NLEEs exhibit richer dynamical behaviors because the varying coefficients can significantly influence wave amplitude, velocity, localization, and interaction properties. The study of exact solutions for these equations is therefore important not only from a mathematical perspective but also for understanding how environmental variations modify nonlinear wave structures. In particular, investigating the integrability conditions of variable-coefficient models provides valuable information about whether fundamental nonlinear structures, such as solitons and breathers, can persist in non-uniform media.

Motivated by these considerations, we investigate a generalized variable-coefficient NLEE that captures the effects of spatial inhomogeneity on nonlinear wave propagation and interaction. In this work, we focus on the following variable-coefficient nonlinear equation:

$$u_{xxxx} + \mathcal{K}_1(y)(u^2)_{xx} + \mathcal{K}_2(y)u_{tt} + \left(\mathcal{K}_3(y)u_t + \mathcal{K}_4(y)u_y + \mathcal{K}_5(y)u_x\right)_x = 0. \tag{1.1}$$

Here, x and y denote the two spatial coordinates, while t represents time. The dependent variable $u = u(x, y, t)$ describes the wave field or wave amplitude in the corresponding two-dimensional spatial domain as it evolves in time. The functions $\mathcal{K}_i(y)$, $i = 1, \ldots, 5$, are variable coefficients. The coefficient $\mathcal{K}_1(y)$ represents the strength of the quadratic nonlinearity, $\mathcal{K}_2(y)$ modulates the temporal dispersive contribution u_{tt}, $\mathcal{K}_3(y)$ and $\mathcal{K}_4(y)$ control the mixed space-time and transverse coupling terms, respectively, whereas $\mathcal{K}_5(y)$ modifies the longitudinal dispersive term u_{xx}. Hence, each variable coefficient corresponds to a spatially varying physical or geometric property of the underlying medium. When all coefficients are constant, Eq (1.1) reduces to the generalized second-order Benjamin–Ono-type equation studied in [33]. By swapping y and t and setting $\mathcal{K}_1(y) = 3$, $\mathcal{K}_2(y) = 3\sigma$, $\mathcal{K}_4(y) = 1$, and $\mathcal{K}_3(y) = \mathcal{K}_5(y) = 0$ with $\sigma^2 = \pm 1$, the equation transforms into the Kadomtsev–Petviashvili (KP) equation. Introduced in 1970, the KP equation generalizes the Korteweg-de Vries (KdV) model to two dimensions, describing small-amplitude ion-acoustic waves in plasmas and finding applications in shallow-water waves, nonlinear optics, plasma physics, Bose-Einstein condensates, and sound propagation in ferromagnetic media [34, 35]. The KP equation is integrable and can be solved via methods such as the inverse scattering transform, Hirota bilinear method, and Darboux transformation. Other reductions of Eq (1.1) reproduce well-known models. Setting $\mathcal{K}_1(y) = $ constant, $\mathcal{K}_2(y) = 1$, and $\mathcal{K}_3(y) = \mathcal{K}_4(y) = \mathcal{K}_5(y) = 0$ yields the second-order Benjamin–Ono equation, which is Painlevé-integrable [36] and admits N-soliton solutions [37]. This equation has been explored via conservation law reductions, Lenard recursion hierarchies [38], and algebro-geometric solutions using theta functions [39], while rogue wave, breather, and lump solutions have been analyzed through homoclinic/heteroclinic limits, Hirota's method, and perturbation techniques [40, 41]. Similarly, choosing $\mathcal{K}_1(y)$, $\mathcal{K}_5(y) = $ constants, $\mathcal{K}_2(y) = 1$, and $\mathcal{K}_3(y) = \mathcal{K}_4(y) = 0$ reduces Eq (1.1) to the classical Boussinesq equation. Formulated in 1871 to model long waves in shallow water, this integrable system supports soliton solutions via the inverse scattering transform and has relevance in describing nonlinear string vibrations and one-dimensional lattice waves [42–45].

Given these connections, it is expected that Eq (1.1) will have applications in oceanography, fluid dynamics, and nonlinear wave theory. Although Painlevé and Hirota-based approaches have been widely used for NLEEs, the novelty of this work lies in establishing the specific integrability conditions of Eq (1.1) and showing that two independent analyses lead to the same result. Through Painlevé analysis, we demonstrate that the equation possesses the Painlevé property within the Set 4 branch when $\mathcal{K}_1(y)$ and $\mathcal{K}_2(y)$ are constants. Under exactly the same conditions, the equation admits explicitly verified one-, two-, three-, and four-soliton solutions, whose pairwise factorization structure motivates a proposed general N-soliton representation. The remaining variable coefficients are retained in the Set 4 Painlevé-compatible equation and enter the wave phases explicitly, allowing us to examine how coefficient variations affect wave propagation and interaction patterns while preserving the soliton structure. Furthermore, we employ the Hirota bilinear method to derive a variety of solutions, including breather waves, lump solutions, and hybrid lump–soliton waves, and investigate their interactions. Graphical comparisons between constant- and variable-coefficient cases further illustrate the distinct wave dynamics generated by different coefficient profiles. Throughout the paper, all graphical results are presented in dimensionless variables. Accordingly, the axes in all figures are labeled by the independent variables x, y, and t, and the dependent variable u, without physical units. The structure of this paper is as follows: Section 2 addresses the Painlevé analysis of Eq (1.1). Section 3 derives the one-, two-, three-, and four-soliton solutions and presents a proposed general N-soliton form. In Section 4, the bilinear form is used to construct breather, lump, and hybrid lump–soliton solutions. Section 5 concludes with a summary of the findings.

2. Integrability in the framework of Painlevé analysis

Painlevé analysis is a method for studying the integrability and singularity behavior of nonlinear differential equations. Named after Paul Painlevé, this technique helps determine if solutions to an equation remain regular and avoid unexpected singularities under certain conditions. It is useful for identifying equations with special solutions that suggest integrability. This analysis is important in fields like physics and engineering for understanding nonlinear systems. In this section, we use the framework from [46] to examine the integrability properties of Eq (1.1). In this context, the term "integrability" refers specifically to the Painlevé property, i.e., the absence of movable critical singularities in the solutions of Eq (1.1). The Painlevé test is a well-known necessary condition for integrability and is widely used to identify equations likely to possess rich mathematical structure. However, it does not by itself guarantee the existence of a Lax pair or other features associated with complete integrability. Consequently, this section focuses solely on determining when Eq (1.1) satisfies the Painlevé property, without claiming full Lax integrability. We explore the possibility that Eq (1.1) admits a Laurent expansion around a singular manifold $\Psi = \Psi(x, y, t)$ in the form

$$u = \sum_{J=0}^{\infty} u_J \Psi^{J+\gamma}, \quad u_0 \neq 0. \tag{2.1}$$

Here, $u_J = u_J(x, y, t)$ and $\Psi = \Psi(x, y, t)$ are analytic functions, and γ denotes a negative integer. The Painlevé test involves three steps: determining the dominant behavior and leading-order coefficient, locating the resonance indices, and checking the compatibility conditions. To determine the leading-order behavior, we consider

$$u = u_0 \Psi^{\gamma}. \tag{2.2}$$

Substituting this expression into Eq (1.1), the dominant contributions arise from the terms u_{xxxx} and $\mathcal{K}_1(y)(u^2)_{xx}$, since they have the lowest powers of Ψ near the singular manifold. The corresponding powers of Ψ are $\gamma - 4$ and $2\gamma - 2$, respectively. Requiring these dominant terms to balance gives

$$\gamma - 4 = 2\gamma - 2, \tag{2.3}$$

which yields $\gamma = -2$. Then, balancing the coefficients of the dominant terms gives

$$120u_0\Psi_x^4 + 20\mathcal{K}_1(y)u_0^2\Psi_x^2 = 0. \tag{2.4}$$

Solving this algebraic equation for the nonzero leading coefficient yields

$$u_0 = -\frac{6}{\mathcal{K}_1(y)}\Psi_x^2, \quad \mathcal{K}_1(y) \neq 0. \tag{2.5}$$

We now determine the resonant indices by perturbing the leading-order solution as

$$u = -\frac{6}{\mathcal{K}_1(y)}\Psi_x^2\Psi^{-2} + u_\jmath\Psi^{\jmath-2}. \tag{2.6}$$

Here, $\jmath$ denotes the resonances related to the dominant behavior γ. By substituting this solution into Eq (1.1) and setting the coefficient of $\Psi^{\jmath-6}$ equal to zero, we obtain

$$(\jmath - 6)(\jmath - 5)(\jmath - 4)(\jmath + 1)u_\jmath\Psi_x^4 = 0. \tag{2.7}$$

Therefore, the resonance points are $\jmath = -1, 4, 5, 6$. As is commonly observed, the resonance at $\jmath = -1$ underscores the inherent ambiguity of the singular manifold $\Psi = 0$. To assess the compatibility conditions, we will analyze the Laurent expansion in Eq (2.1) in the following manner:

$$u = \sum_{\jmath=0}^{6} u_\jmath\Psi^{\jmath-2}. \tag{2.8}$$

By substituting Eq (2.8) into Eq (1.1) and setting the coefficients of $\Psi^{\jmath-6}$ equal to zero, we derive an explicit expression for the non-resonant level in terms of u_1, u_2, and u_3:

$$\begin{aligned}
\Psi^{-5}: \quad & u_1 = \frac{6\Psi_{xx}}{\mathcal{K}_1(y)},\\
\Psi^{-4}: \quad & u_2 = \frac{-\mathcal{K}_5(y)\Psi_x^2 - \mathcal{K}_4(y)\Psi_x\Psi_y - \mathcal{K}_3(y)\Psi_x\Psi_t - \mathcal{K}_2(y)\Psi_t^2 - 4\Psi_x\Psi_{xxx} + 3\Psi_{xx}^2}{2\Psi_x^2\mathcal{K}_1(y)},\\
\Psi^{-3}: \quad & u_3 = \frac{1}{2\Psi_x^4\mathcal{K}_1^2(y)}\Big[\mathcal{K}_1(y)\Big(\Psi_x^2\Psi_{xxxx} - 4\Psi_x\Psi_{xx}\Psi_{xxx} + 3\Psi_{xx}^3 - \Big(\Psi_x\left(\mathcal{K}_4(y)\Psi_y + \mathcal{K}_3(y)\Psi_t\right) + \mathcal{K}_2(y)\Psi_t^2\Big)\Psi_{xx}\Big)\\
& \quad + \Psi_x^2\Big(\mathcal{K}_1(y)(\mathcal{K}_2(y)\Psi_{tt} + \mathcal{K}_3(y)\Psi_{xt} + \mathcal{K}_4(y)\Psi_{xy}) - \mathcal{K}_4(y)\mathcal{K}_{1,y}(y)\Psi_x\Big)\Big],
\end{aligned} \tag{2.9}$$

where $\mathcal{K}_1 \neq 0$. The coefficients of Ψ^{-2} and Ψ^{-1} vanish identically, indicating that u_4 and u_5, respectively, remain arbitrary at the corresponding resonance levels. However, at the resonance point $\jmath = 6$, the recursion relation for u_6 yields a compatibility condition given by

$$\begin{aligned}
&\mathcal{K}_1(y)\left(4\mathcal{K}_{1,y}(y)\mathcal{K}_2(y) - \mathcal{K}_{2,y}(y)\mathcal{K}_1(y)\right)\left(\Psi_x^2\Psi_{tt} - 2\Psi_x\Psi_t\Psi_{tx} + \Psi_t^2\Psi_{xx}\right)\\
&+ \Psi_x^3\left(\mathcal{K}_{4,y}(y)\mathcal{K}_{1,y}(y)\mathcal{K}_1(y) - 3\mathcal{K}_{1,y}^2(y)\mathcal{K}_4(y) + \mathcal{K}_4(y)\mathcal{K}_1(y)\mathcal{K}_{1,yy}(y)\right) = 0.
\end{aligned} \tag{2.10}$$

Since Ψ is arbitrary, the coefficients multiplying the independent structures involving Ψ must vanish separately. Therefore, the compatibility condition requires:

$$\begin{aligned}
&\textbf{Set 1: } \mathcal{K}_1(y) = 0,\\
&\textbf{Set 2: } \mathcal{K}_2(y) = c_1\mathcal{K}_1(y)^4, \;\; \mathcal{K}_4(y) = 0,\\
&\textbf{Set 3: } \mathcal{K}_2(y) = c_2\mathcal{K}_1(y)^4, \;\; \mathcal{K}_4(y) = \frac{c_3\mathcal{K}_1(y)^3}{\mathcal{K}_1(y)_y},\\
&\textbf{Set 4: } \mathcal{K}_1(y) = c_4, \;\; \mathcal{K}_2(y) = c_5,
\end{aligned} \tag{2.11}$$

where c_i, $i = 1, \dots, 5$, are constants and $\mathcal{K}_1 \neq 0$. The four sets above represent different possibilities for satisfying the Painlevé compatibility condition. However, Set 1 requires special consideration. The derivation of the leading-order coefficient Eq (2.5) already assumes $\mathcal{K}_1(y) \neq 0$. Therefore, the case where $\mathcal{K}_1(y) = 0$ does not belong to the nonlinear Painlevé branch analyzed above. Instead, it corresponds to a separate linear reduction in which the nonlinear term $(u^2)_{xx}$ vanishes. Consequently, Set 1 should be regarded as a degenerate linear case rather than a nonlinear Painlevé-integrable case.

Furthermore, Sets 2 and 3 preserve the nonlinear structure of Eq (1.1), but they impose specific functional relationships among the variable coefficients, namely, $\mathcal{K}_1(y)$, $\mathcal{K}_2(y)$, and $\mathcal{K}_4(y)$. Therefore, these cases correspond to constrained variable-coefficient integrable subclasses rather than the most general form of the model. Such reductions may possess their own exact solutions and integrable structures; however, their investigation is beyond the scope of the present study. In contrast, Set 4 retains the nonlinear term while assigning constant coefficients to the dominant nonlinear and temporal-dispersive contributions. We therefore focus on Set 4 and obtain the following Painlevé-compatible form studied in the remainder of the paper:

$$u_{xxxx} + C_1(u^2)_{xx} + C_2u_{tt} + \mathcal{K}_3(y)u_{xt} + \mathcal{K}_4(y)u_{xy} + \mathcal{K}_5(y)u_{xx} = 0, \tag{2.12}$$

where C_1 and C_2 are constant coefficients. The present analysis assumes that the coefficients $\mathcal{K}_i$ depend only on y. Extending the calculation to coefficients depending on t, or jointly on (t, y), may produce different compatibility conditions and lies beyond the scope of this study. We now demonstrate that the Set 4 Painlevé-compatible equation given in Eq (2.12) can be transformed into a Hirota bilinear form. To this end, we recall the definition of the Hirota bilinear operator [47]. For two sufficiently differentiable functions f and g, the Hirota operator is defined by

$$D_x^m D_y^n D_t^p (f \cdot g) = (\partial_x - \partial_{x'})^m (\partial_y - \partial_{y'})^n (\partial_t - \partial_{t'})^p f(x, y, t) g(x', y', t')\big|_{x'=x,\, y'=y,\, t'=t}, \tag{2.13}$$

where m, n, and p are nonnegative integers. In particular, the fourth-order x-derivative satisfies the identity

$$\frac{D_x^4 \xi \cdot \xi}{2\xi^2} = (\ln \xi)_{xxxx} + 6(\ln \xi)_{xx}^2. \tag{2.14}$$

This identity is consistent with the structure of Eq (2.12), which contains the fourth-order term u_{xxxx} and the nonlinear term $(u^2)_{xx}$. Therefore, we introduce the dependent-variable transformation

$$u = R(\ln \xi)_{xx}, \tag{2.15}$$

where $\xi = \xi(x, y, t)$ is an auxiliary function and R is a constant to be determined. The choice $u \propto (\ln \xi)_{xx}$ allows the linear and nonlinear terms of the equation to be expressed through the same Hirota structure.

To determine the dispersion relation, we first consider the linear part of Eq (2.12) and use the exponential trial function

$$u = \mathrm{e}^{h_i x + q_i(y) + w_i t + \zeta_i}, \tag{2.16}$$

where h_i, w_i, and ζ_i are arbitrary constants, while $q_i\,(y)$ is an unknown function of y to be determined. Afterward, we solve the resulting equation to obtain the dispersion relation, which is expressed as

$$q_i(y) = -\int \left(\frac{h_i^4 + w_i^2 C_2 + w_i h_i \mathcal{K}_3(y) + h_i^2 \mathcal{K}_5(y)}{h_i \mathcal{K}_4(y)} \right) dy, \tag{2.17}$$

where $h_i \neq 0$ and $K_4(y) \neq 0$. Consequently, the dispersion variable can be written as

$$\Theta_i = h_i x - \int \left(\frac{h_i^4 + w_i^2 C_2 + w_i h_i \mathcal{K}_3(y) + h_i^2 \mathcal{K}_5(y)}{h_i \mathcal{K}_4(y)} \right) dy + w_i t + \zeta_i. \tag{2.18}$$

Next, substituting the transformation Eq (2.15) into Eq (2.12) along with

$$\xi = 1 + e^{\Theta_i}, \tag{2.19}$$

and solving for R, we find that $R = \frac{6}{C_1}$. Consequently, the dependent-variable transformation becomes

$$u = \frac{6}{C_1} (\ln \xi)_{xx}. \tag{2.20}$$

Substituting Eq (2.20) into Eq (2.12) and integrating twice with respect to x, we impose the localized/decaying boundary conditions used for the wave solutions considered here. Under these conditions, the two functions of integration depending on (y, t) vanish, and we obtain

$$(\xi_{xxxx}\xi - 4\xi_{xxx}\xi_x + 3\xi_{xx}^2) + C_2(\xi_{tt}\xi - \xi_t^2) + \mathcal{K}_3(y)(\xi\xi_{xt} - \xi_t\xi_x) + \mathcal{K}_4(y)(\xi_{xy}\xi - \xi_x\xi_y) + \mathcal{K}_5(y)(\xi_{xx}\xi - \xi_x^2) = 0, \tag{2.21}$$

which can be written in the following compact form by utilizing the definition of the Hirota bilinear operator given in Eq (2.13):

$$(D_x^4 + C_2 D_t^2 + \mathcal{K}_3(y) D_x D_t + \mathcal{K}_4(y) D_x D_y + \mathcal{K}_5(y) D_x^2)\xi.\xi = 0. \tag{2.22}$$

This equation represents the bilinear form of the Set 4 Painlevé-compatible Eq (2.12). We remark that the bilinear equation given in Eq (2.22) can also be derived by means of the Bell polynomial method [48]. In this approach, motivated by the leading-order analysis in the Painlevé test, one introduces the dependent-variable transformation $u = \frac{6}{C_1} q_{xx}$, where $q = q(x, y, t)$. Integrating the resulting equation twice with respect to x and imposing the same localized/decaying boundary conditions makes the two functions of integration depending on (y, t) vanish. The resulting equation can then be expressed in terms of the P-polynomials. By exploiting the correspondence between the Bell P-polynomials and Hirota bilinear operators, the bilinear form Eq (2.22) is obtained directly. The compatibility analysis identifies several branches. In the remainder of this work, we focus on the Set 4 branch, for which $\mathcal{K}_1(y) = C_1$ and $\mathcal{K}_2(y) = C_2$. We next examine the explicitly constructed multi-soliton solutions under these same coefficient conditions.

3. Existence of soliton solutions

In integrable-systems theory, the existence of multi-soliton solutions with factorized interactions is commonly regarded as an important indicator of an underlying integrable structure, often associated with conservation laws, symmetry hierarchies, or inverse-scattering formulations [49]. In this section, we use soliton solutions as a constructive indicator of integrability, in the same spirit as the Painlevé analysis, which provides a singularity-based indicator. More precisely, we explicitly construct and verify one-, two-, three-, and four-soliton solutions under the Set 4 coefficient conditions obtained from the Painlevé analysis. Their agreement provides mutually consistent evidence for a special class of the equation possessing the Painlevé property and supporting multi-soliton structures.

The single-soliton solution is taken to be

$$u = R(\ln \xi_1)_{xx}, \tag{3.1}$$

where R is a real parameter, and the auxiliary function $\xi_1(x, y, t)$ is defined as

$$\xi_1 = 1 + e^{\Theta_1}, \tag{3.2}$$

with the phase variable Θ_1 defined by

$$\Theta_1 = h_1 x - \int \left(\frac{h_1^4 + w_1^2 \mathcal{K}_2(y) + w_1 h_1 \mathcal{K}_3(y) + h_1^2 \mathcal{K}_5(y)}{h_1 \mathcal{K}_4(y)} \right) dy + w_1 t + \zeta_1, \tag{3.3}$$

where $h_1 \neq 0$ and $\mathcal{K}_4(y) \neq 0$ throughout the domain considered. Substituting Eq (3.2) into Eq (1.1) and solving for R, we find that $R = \frac{6}{\mathcal{K}_1(y)}$. To determine a constant value for R, we impose the coefficient condition

$$\mathcal{K}_1(y) = C_1, \tag{3.4}$$

where C_1 is a real constant. The constraint in Eq (3.4) is part of the Set 4 conditions obtained from the Painlevé analysis. We will show that, together with $\mathcal{K}_2(y) = C_2$, it supports the explicitly constructed one-, two-, three-, and four-soliton solutions and the proposed general N-soliton structure. The single-soliton solution is obtained by substituting Eq (3.2) into Eq (3.1) and applying the condition in Eq (3.4) as follows:

$$u = \frac{6h_1^2 e^{\Theta_1}}{C_1(1 + e^{\Theta_1})^2}. \tag{3.5}$$

The signed extremal value of the one-soliton solution is $\frac{3h_1^2}{2C_1}$, while its absolute amplitude is $\frac{3h_1^2}{2|C_1|}$. Hence, the amplitude is independent of the coefficients $\mathcal{K}_i(y)$, $i = 2, \ldots, 5$. For centuries, water waves have captivated the interest of mathematicians, physicists, and engineers. While the ocean hosts numerous wave types, this study specifically examines solitary waves, oceanic solitons, and localized waves in shallow water. To demonstrate the single-soliton solution, we analyze various variable coefficients and parameter choices, revealing a range of physical structures, as depicted in Figure 1. When the variable coefficients are chosen as constants (Figure 1(a)), the resulting solution forms a bell-shaped solitary wave. However, when the coefficients are selected as functions of y, the resulting solutions produce different wave forms, such as periodic (Figure 1(b)), curved (Figure 1(c)), and V-shaped (Figure 1(d)) waves. In all scenarios, the wave amplitude remains unchanged because it is independent of the variable coefficients. These different wave profiles demonstrate that the variable coefficients mainly influence the propagation characteristics rather than the amplitude of the solitary wave. In particular, $\mathcal{K}_3(y)$ modifies the propagation direction through the mixed space-time coupling, $\mathcal{K}_4(y)$ governs the transverse phase evolution and consequently changes the wave trajectory, while $\mathcal{K}_5(y)$ alters the effective dispersive properties, producing curved or periodically modulated wave fronts. Thus, within the plotted parameter sets, the variable coefficients modify the geometry and trajectory of the localized wave while leaving its analytical peak magnitude unchanged.

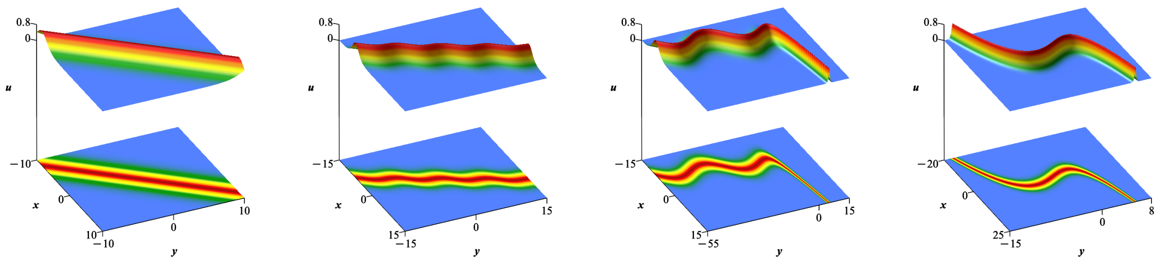

(a) (b) (c) (d)

Figure 1. Evolution of the one-soliton wave Eq (3.5). The plots show the corresponding solution $u(x,y,t)$ with $t = 0$. The common parameters are $h_1 = 1$, $w_1 = \frac{1}{5}$, $\zeta_1 = 0$, $C_1 = 2$, $C_2 = 1$. The parameters used for each panel are: **(a)** $\mathcal{K}_3(y) = 2$, $\mathcal{K}_4(y) = 3$, $\mathcal{K}_5(y) = 1$, **(b)** $\mathcal{K}_3(y) = 2$, $\mathcal{K}_4(y) = 3$, $\mathcal{K}_5(y) = \sin\left(\frac{4y}{5}\right)$, **(c)** $\mathcal{K}_3(y) = \sin(\frac{y}{5})$, $\mathcal{K}_4(y) = \frac{1}{2}$, $\mathcal{K}_5(y) = \tanh\left(\frac{y}{3}\right)$, and **(d)** $\mathcal{K}_3(y) = \frac{y}{5}$, $\mathcal{K}_4(y) = \frac{1}{y}$, $\mathcal{K}_5(y) = \tanh\left(\frac{y}{5}\right)$.

For the two-soliton solutions, we introduce the auxiliary function

$$\xi_2(x,y,t) = 1 + e^{\Theta_1} + e^{\Theta_2} + \mathcal{A}_{12}e^{\Theta_1+\Theta_2}. \tag{3.6}$$

Here, the arguments Θ_i are given by

$$\Theta_i = h_i x - \int \left(\frac{h_i^4 + w_i^2\mathcal{K}_2(y) + w_i h_i \mathcal{K}_3(y) + h_i^2\mathcal{K}_5(y)}{h_i\mathcal{K}_4(y)} \right) dy + w_i t + \zeta_i, \quad i = 1,2. \tag{3.7}$$

By substituting

$$u = \frac{6}{C_1}(\ln \xi_2)_{xx}, \tag{3.8}$$

along with Eq (3.6) into Eq (1.1) and solving for the phase shift $\mathcal{A}_{12}$, we derive

$$\mathcal{A}_{12} = \frac{-\mathcal{K}_2(y)(h_1w_2 - h_2w_1)^2 + 3h_2^2h_1^2(h_1 - h_2)^2}{-\mathcal{K}_2(y)(h_1w_2 - h_2w_1)^2 + 3h_2^2h_1^2(h_1 + h_2)^2}. \tag{3.9}$$

The two-soliton solution is then derived. To satisfy solution Eq (3.8) in the main Eq (1.1), the following condition must be applied to the solution:

$$\mathcal{K}_2(y) = C_2, \tag{3.10}$$

where C_2 is a real constant. The conditions in Eqs (3.4) and (3.10) constitute the coefficient restrictions used for the Set 4 soliton construction identified in Eq (2.11). The two-soliton solution for various choices of variable parameters is shown in Figure 2. In all instances, the largest wave has an amplitude of $\frac{1}{12}$, while the smallest wave has an amplitude of $\frac{3}{64}$. In Figure 2(a), the plotted profiles merge and subsequently separate. Figure 2(b) exhibits a more curved interaction pattern for $\mathcal{K}_3(y) = \sin^2\left(\frac{y}{3}\right)$. Figure 2(c) shows additional periodic modulation for $\mathcal{K}_3(y) = 4\cos(5y)$, whereas Figure 2(d) displays a strongly asymmetric profile for $\mathcal{K}_3(y) = \frac{y}{4}$. These plots illustrate changes in waveform geometry and trajectory under the stated coefficient choices; they do not, by themselves, establish stability or energy-transfer properties.

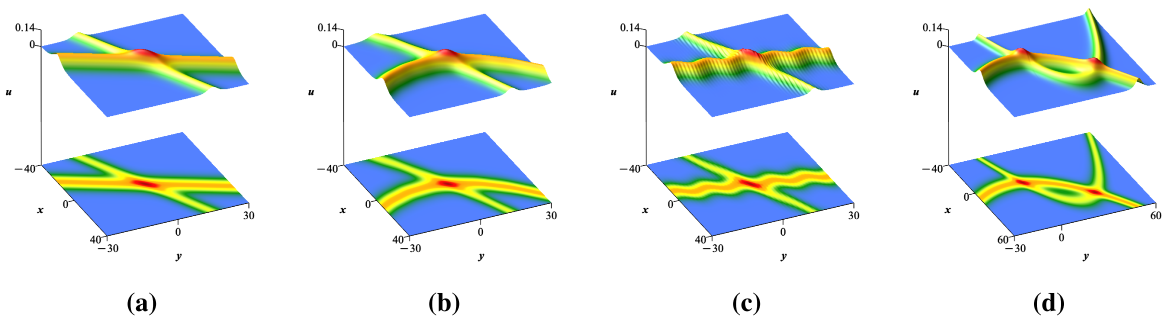

Figure 2. Evolution of the two-soliton wave Eq (3.8). The plots show the corresponding solution $u(x, y, t)$ with $t = 0$. The common parameters are $h_1 = \frac{1}{3}$, $h_2 = -\frac{1}{4}$, $w_1 = \frac{1}{5}$, $w_2 = \frac{1}{2}$, $\zeta_1 = \zeta_2 = 0$, $C_1 = 2$, $C_2 = 3$, $\mathcal{K}_4(y) = 4$. The parameters used for each panel are: **(a)** $\mathcal{K}_3(y) = 1$, $\mathcal{K}_5(y) = 1$, **(b)** $\mathcal{K}_3(y) = \sin^2\left(\frac{y}{3}\right), \mathcal{K}_5(y) = \frac{y}{6}$, **(c)** $\mathcal{K}_3(y) = 4\cos(5y)$, $\mathcal{K}_5(y) = 3\cos\left(\frac{y}{2}\right)$, and **(d)** $\mathcal{K}_3(y) = \frac{y}{4}$, $\mathcal{K}_5(y) = \sin(e^y)$.

For the three-soliton solutions, we define the auxiliary function as

$$\xi_3 = 1 + e^{\Theta_1} + e^{\Theta_2} + e^{\Theta_3} + \mathcal{A}_{12}e^{\Theta_1+\Theta_2} + \mathcal{A}_{13}e^{\Theta_1+\Theta_3} + \mathcal{A}_{23}e^{\Theta_2+\Theta_3} + \mathcal{A}_{123}e^{\Theta_1+\Theta_2+\Theta_3}. \tag{3.11}$$

By substituting

$$u = \frac{6}{C_1}(\ln \xi_3)_{xx}, \tag{3.12}$$

along with Eq (3.11) into Eq (1.1), we obtain

$$\mathcal{A}_{123} = \mathcal{A}_{12}\mathcal{A}_{13}\mathcal{A}_{23}, \tag{3.13}$$

where Θ_j are given in Eq (3.7) and

$$\mathcal{A}_{ij} = \frac{-C_2(h_i w_j - h_j w_i)^2 + 3h_j^2 h_i^2 (h_i - h_j)^2}{-C_2(h_i w_j - h_j w_i)^2 + 3h_j^2 h_i^2 (h_i + h_j)^2}. \tag{3.14}$$

As in the two-soliton case, the three-soliton solution satisfies Eq (1.1) under the coefficient condition in Eq (3.10). This calculation establishes the two- and three-soliton cases. Together with the verified one- and four-soliton solutions, it provides supporting evidence for the proposed general

N-soliton structure. The physical representation of the three-soliton solution is shown in Figure 3, with different parameter values. Figure 3(a) exhibits sharp peaks and steep wavefronts. Figure 3(b) shows a curved, periodically modulated profile for the stated sinusoidal coefficient choice. Figure 3(c) contains multiple overlapping peaks when $\mathcal{K}_5(y) = 3\cos\left(\frac{y}{2}\right)$, while Figure 3(d) presents a stretched and asymmetric profile for $\mathcal{K}_5(y) = 2\tanh\left(\frac{y}{3}\right)$. These visualizations demonstrate coefficient-dependent changes in propagation geometry and interaction patterns without making a separate claim about dynamical stability or energy exchange.

The identity $\mathcal{A}_{123} = \mathcal{A}_{12}\mathcal{A}_{13}\mathcal{A}_{23}$ shows that the verified three-soliton interaction factorizes into pairwise interactions. This is the characteristic three-soliton condition used in Hirota's direct method [47]. Based on the explicitly verified one-, two-, three-, and four-soliton cases and this pairwise factorization property, we propose the following N-soliton form for $N > 1$ under the conditions $\mathcal{K}_1(y) = C_1$ and $\mathcal{K}_2(y) = C_2$. Although the expression follows the standard Hirota binary-sum structure, a complete proof for arbitrary N is beyond the scope of the present work:

$$u = \frac{6}{C_1}(\ln \xi_N)_{xx}, \tag{3.15}$$

where

$$\xi_N = \sum_{\tau=0,1} \exp\left(\sum_{i=1}^{N} \tau_i \Theta_i + \sum_{i<j}^{N} \tau_i \tau_j \ln(\mathcal{A}_{i,j})\right). \tag{3.16}$$

Here, the notation $\sum_{\tau=0,1}$ denotes the summation over all possible combinations of $\tau_i = 0, 1$ for $i = 1, 2, \ldots, N$. The phase variables Θ_i are given in Eq (3.7) and the interaction coefficients $\mathcal{A}_{i,j}$ are defined in Eq (3.14).

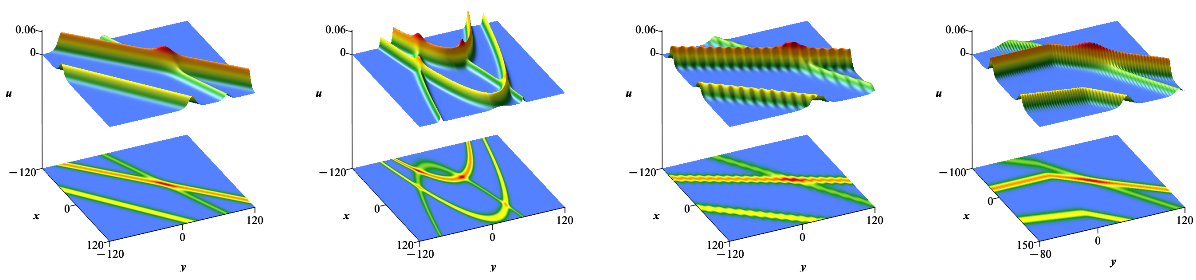

(a) (b) (c) (d)

Figure 3. Evolution of the three-soliton wave Eq (3.12). The plots show the corresponding solution $u(x, y, t)$ with $t = 0$. The common parameters are $h_1 = -\frac{1}{4}$, $h_2 = -\frac{1}{5}$, $h_3 = \frac{1}{7}$, $w_1 = \frac{1}{5}$, $w_2 = 2$, $w_3 = -\frac{1}{3}$, $\zeta_1 = -7$, $\zeta_2 = 20$, $\zeta_3 = 10$, $C_1 = 2$, $C_2 = 3$, $\mathcal{K}_4(y) = 4$. The parameters used for each panel are: **(a)** $\mathcal{K}_3(y) = 1$, $\mathcal{K}_5(y) = 3$, **(b)** $\mathcal{K}_3(y) = \frac{y}{4}$, $\mathcal{K}_5(y) = \sin(e^y)$, **(c)** $\mathcal{K}_3(y) = 4\cos(5y)$, $\mathcal{K}_5(y) = 3\cos\left(\frac{y}{2}\right)$, and **(d)** $\mathcal{K}_3(y) = 3\sin(2y)$, $\mathcal{K}_5(y) = 2\tanh\left(\frac{y}{3}\right)$.

Setting $N = 4$ in the proposed form Eq (3.15) gives the four-soliton expression. We have directly verified the four-soliton solution by substituting it into Eq (1.1). The resulting expression satisfies the equation identically under the conditions $\mathcal{K}_1(y) = C_1$ and $\mathcal{K}_2(y) = C_2$. This verification, together with the previously obtained two- and three-soliton solutions, provides further support for the pairwise interaction structure and verifies the $N = 4$ case of Eq (3.15). Figure 4 illustrates four-soliton profiles under different coefficient choices. Figure 4(a) contains multiple sharp and overlapping peaks. Figure 4(b) exhibits a periodically modulated structure, Figure 4(c) shows a strongly curved profile, and Figure 4(d) displays a stretched and asymmetric configuration. These plots demonstrate coefficient-dependent changes in waveform geometry and spatial organization but do not independently establish collision dynamics, stability, or shape preservation.

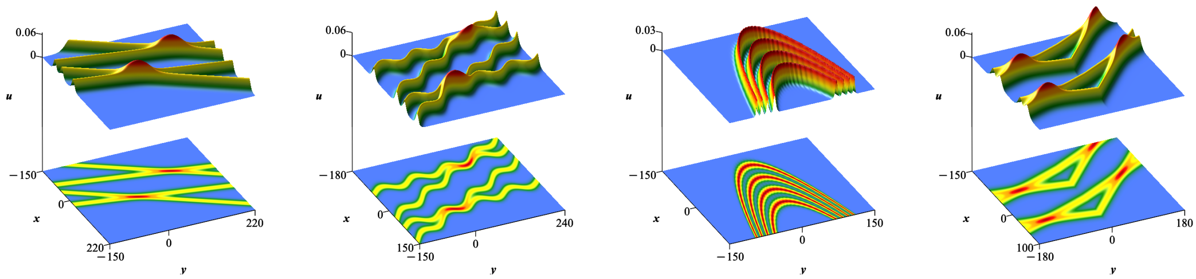

(a) **(b)** **(c)** **(d)**

Figure 4. Evolution of the four-soliton wave. The plots show the corresponding solution $u(x, y, t)$ with $t = 0$. The common parameters are $h_1 = -\frac{1}{5}$, $h_2 = -\frac{1}{5}$, $h_3 = \frac{1}{5}$, $h_4 = \frac{1}{5}$, $w_1 = -\frac{1}{6}$, $w_2 = 2$, $w_3 = -\frac{1}{3}$, $w_4 = \frac{2}{5}$, $\zeta_1 = -20$, $C_1 = 2$, $C_2 = -2$, $\mathcal{K}_4(y) = 4$. The parameters used for each panel are: **(a)** $\zeta_2 = 10$, $\mathcal{K}_3(y) = 1$, $\mathcal{K}_5(y) = 3$, **(b)** $\zeta_2 = 10$, $\mathcal{K}_3(y) = 1$, $\mathcal{K}_5(y) = 3\cos\left(\frac{y}{15}\right)$, **(c)** $\zeta_2 = 0$, $\mathcal{K}_3(y) = 3\sin(y)$, $\mathcal{K}_5(y) = \frac{y}{5}$, and **(d)** $\zeta_2 = 0$, $\mathcal{K}_3(y) = \tanh(y)$, $\mathcal{K}_5(y) = -\tanh(y)$.

We conclude that the Painlevé analysis and the explicitly verified one-, two-, three-, and four-soliton solutions provide mutually consistent evidence for the special mathematical structure of the variable-coefficient equation under the Set 4 conditions. The proposed general N-soliton form is supported by the observed pairwise factorization property and the direct verification of the four-soliton case, but it has not been proved for arbitrary N. These results are understood in the Painlevé and soliton senses and do not constitute a proof of complete Lax integrability. Henceforth, we focus on the resulting Eq (2.12). It should be noted that the conditions $\mathcal{K}_1(y) = C_1$ and $\mathcal{K}_2(y) = C_2$ characterize the Set 4 Painlevé branch and the corresponding N-soliton structure investigated in this work. Although other Painlevé-compatible subclasses, such as Sets 2 and 3, may exist, they correspond to different constrained variable-coefficient structures and are not considered further here. Other coefficient choices may still allow particular exact or localized solutions under suitable restrictions. A systematic classification of such solutions remains an interesting direction for future work.

4. Exact solutions via the ansatz method

The ansatz method is a widely used technique for finding exact solutions to NLEEs. It begins with an educated assumption about the solution's form, guided by the equation's symmetry and structure. By substituting this assumed solution into the transformed or bilinear form of the equation, the complexity of the original problem is significantly reduced. This substitution often yields a set of solvable algebraic or lower-order differential equations, enabling the determination of key parameters. Once a solution is obtained, it is validated by reintroducing it into the original equation to confirm its accuracy. This approach is particularly useful in the study of nonlinear wave dynamics, as it not only simplifies intricate mathematical problems, but also reveals fundamental properties of solitons, rogue waves, and other complex wave phenomena. Below, we define the test function ξ to derive a broad class of exact solutions to Eq (2.12). All solutions presented in this section were checked by direct symbolic substitution into both the bilinear equation given in Eq (2.22) and the original nonlinear equation (2.12), after imposing the stated parameter restrictions. In each case, the corresponding residual simplifies identically to zero.

4.1. Breather wave

To construct breather-wave solutions of Eq (2.12), we employ the dependent-variable transformation $u = \frac{6}{C_1}(\ln\xi)_{xx}$, where the auxiliary function ξ is defined as follows:

$$\xi = \mathrm{e}^{-\lambda\theta_1} + \delta_1\mathrm{e}^{\lambda\theta_1} + \delta_2\cos(\beta\theta_2), \tag{4.1}$$

where, $\theta_1 = x + a_1\omega_1(y) + a_2t + a_3$ and $\theta_2 = x + b_1\omega_2(y) + b_2t + b_3$. The parameters λ, β, δ_1, δ_2, a_i, and b_i, $i = 1, 2, 3$, and functions $\omega_1(y)$ and $\omega_2(y)$ are unknown and need to be determined. By substituting the test function Eq (4.1) into the bilinear Eq (2.22) and setting all the coefficients of $\mathrm{e}^{\pm\lambda\theta_1}$, $\cos(\beta\theta_2)$, and $\sin(\beta\theta_2)$ to zero, we obtain a system of equations. Solving this system yields

$$\begin{aligned}
\omega_1(y) &= -\int \frac{\beta^2C_2b_2(2a_2-b_2)+\beta^2(a_2\mathcal{K}_3(y)-3\beta^2+\mathcal{K}_5(y)-2\lambda^2)+\lambda^2(a_2\mathcal{K}_3(y)+C_2a_2^2+\mathcal{K}_5(y)+1)}{a_1\mathcal{K}_4(y)(\beta^2+\lambda^2)}\,dy,\\
\omega_2(y) &= -\int \frac{C_2\beta^2b_2^2+\beta^2(b_2\mathcal{K}_3(y)-\beta^2+\mathcal{K}_5(y)+2\lambda^2)+\lambda^2(b_2\mathcal{K}_3(y)-C_2a_2^2+\mathcal{K}_5(y)+2a_2b_2C_2+3\lambda^2)}{b_1\mathcal{K}_4(y)(\beta^2+\lambda^2)}\,dy,\\
\delta_1 &= -\frac{\beta^2\delta_2^2\left((\beta^2+\lambda^2)^2-\frac{\lambda^2C_2(a_2-b_2)^2}{3}\right)}{4\lambda^2\left((\beta^2+\lambda^2)^2+\frac{\beta^2C_2(a_2-b_2)^2}{3}\right)}.
\end{aligned} \tag{4.2}$$

For the breather solution, all parameters are chosen so that the expressions in Eq (4.2) are real and well-defined. In particular, $\lambda, \beta, a_1, b_1 \neq 0$, $\mathcal{K}_4(y) \neq 0$ throughout the domain, and $\beta^2 + \lambda^2 > 0$. Moreover, the denominator in the expression for δ_1 must not vanish; hence,

$$C_2 \neq -\frac{3\left(\beta^2+\lambda^2\right)^2}{\beta^2\left(a_2-b_2\right)^2}, \tag{4.3}$$

whenever $a_2 \neq b_2$. The remaining parameters and functions of y may be selected freely subject to these restrictions and to the requirement that every displayed square root, logarithm, or denominator be real and nonzero. The integrals in Eq (4.2) are understood as y-integrals over intervals on which their integrands are finite, with arbitrary constants of integration absorbed into the phase parameters. By substituting these results back into the test function Eq (4.1) and applying the logarithmic transformation Eq (2.20), we obtain the breather solution. The resulting auxiliary function ξ is then substituted into the bilinear equation given in Eq (2.22), and the corresponding residual vanishes identically, confirming the validity of the solution. Through the transformation, this also verifies that the obtained breather solution satisfies Eq (2.12).

Breather solutions are important in many areas of physics and applied mathematics, such as optics, condensed matter physics, and fluid dynamics. They have been observed in various physical systems, like optical fibers and other wave-propagating media [50, 51]. The study of breather solutions provides insight into nonlinear wave phenomena, particularly in understanding how energy can be confined and sustained within localized structures in a larger wave environment. These solutions are essential for investigating situations where localized, periodic disturbances can persist and influence the system's overall behavior. In Figure 5, the breather solution is shown with the corresponding parameters chosen. Variations in parameters influence the shape, amplitude, periodicity, and localization of the breathers. These breathers are localized oscillatory structures that preserve their shape as they propagate, typically emerging from a balance between nonlinearity and dispersion. While some breathers remain symmetric (Figure 5(a)), others become skewed or tilted (Figure 5(b)–(d)), revealing directional propagation and the effects of the underlying parameters.

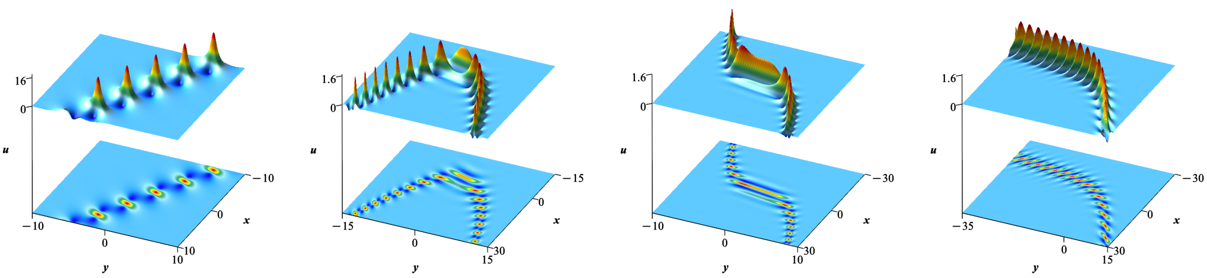

(a) **(b)** **(c)** **(d)**

Figure 5. Evolution of the breather wave Eq (4.1). The plots show the corresponding solution $u(x, y, t)$ with $t = 0$. The common parameters are $\beta = 1$, $\lambda = -\frac{1}{2}$, $\delta_2 = \frac{2}{5}$, $a_2 = 2$, $a_3 = \frac{1}{3}$, $b_2 = -1$, $b_3 = 0$, $C_2 = -1$. The parameters used for each panel are: **(a)** $C_1 = 1$, $\mathcal{K}_3(y) = \frac{5}{2}$, $\mathcal{K}_4(y) = -10$, $\mathcal{K}_5(y) = 1$, **(b)** $C_1 = 4$, $\mathcal{K}_3(y) = \frac{3y}{5}$, $\mathcal{K}_4(y) = 3$, $\mathcal{K}_5(y) = \cos(\frac{y}{2})$, **(c)** $C_1 = 4$, $\mathcal{K}_3(y) = \frac{y^2}{5}$, $\mathcal{K}_4(y) = 3$, $\mathcal{K}_5(y) = \cos\left(\frac{y}{10}\right)$, and **(d)** $C_1 = 4$, $\mathcal{K}_3(y) = 2$, $\mathcal{K}_4(y) = 3$, $\mathcal{K}_5(y) = 4\tanh\left(\frac{y}{10}\right)$.

Figure 5(a) shows a symmetric profile with periodic peaks in both spatial directions. In Figure 5(b), the peaks are shifted, and the plotted amplitude is reduced, producing a V-shaped wavefront. Figure 5(c) displays an elongated and tilted profile under cosine modulation, while Figure 5(d) shows a more directional, tilted wave packet for the stated hyperbolic-tangent coefficient. These descriptions concern the geometry of the exact plotted solutions and do not constitute an independent stability or energy analysis. The coefficients of the selected variables directly influence the propagation and localization of the breather wave. In particular, the coefficient $\mathcal{K}_3(y)$ modifies the coupling between the spatial and temporal derivatives and therefore affects the direction of propagation and wave tilt. The choice of $\mathcal{K}_4(y)$ controls the accumulation of phases dependent on y, leading to changes in the orientation and spatial location of the breather. Meanwhile, $\mathcal{K}_5(y)$ modifies the dispersive contribution and can introduce additional modulation of the wave profile. Thus, the different coefficient choices in Figure 5 produce symmetric, skewed, or tilted breathers while preserving their localized oscillatory character.

4.2. Lump wave

The following quadratic function is applied to derive the lump solution $u = \frac{6}{C_1}(\ln \xi)_{xx}$.

$$\xi = (a_1 x + a_2\omega_1(y) + a_3 t + a_4)^2 + (a_5 x + a_6\omega_2(y) + a_7 t + a_8)^2 + a_9, \tag{4.4}$$

where parameters a_i, $i = 1, \ldots, 9$, and functions $\omega_1(y)$ and $\omega_2(y)$ are initially undetermined and must be determined. By substituting this function into Eq (2.22) and solving for the unknown constants, we obtain the following results:

$$\begin{aligned}
\omega_1(y) &= -\int \frac{a_1 C_2(a_3^2 - a_7^2) + a_3(a_1^2\mathcal{K}_3(y) + a_5^2\mathcal{K}_3(y) + 2a_5 a_7 C_2) + a_1\mathcal{K}_5(y)(a_1^2 + a_5^2)}{a_2\mathcal{K}_4(y)(a_1^2 + a_5^2)}\, dy,\\
\omega_2(y) &= -\int \frac{C_2(2a_1 a_3 a_7 - a_5 a_3^2 + a_5 a_7^2) + a_7\mathcal{K}_3(y)(a_1^2 + a_5^2) + a_5\mathcal{K}_5(y)(a_1^2 + a_5^2)}{a_6\mathcal{K}_4(y)(a_1^2 + a_5^2)}\, dy,\\
a_9 &= -\frac{3\left(a_1^2 + a_5^2\right)^3}{C_2\,(a_1 a_7 - a_3 a_5)^2}.
\end{aligned} \tag{4.5}$$

For the lump solution to be a regular real solution, it is necessary that $\xi > 0$ throughout the considered domain. Since ξ is the sum of two squares and the constant a_9, this requires $a_9 > 0$. From Eq (4.5), this condition implies $C_2 < 0$, provided $a_1 a_7 - a_3 a_5 \neq 0$. Therefore, in this family of solutions, $\mathcal{K}_4(y)$ and the parameters C_2, a_2, and a_6 are nonzero. Moreover, $(a_1, a_5) \neq (0, 0)$, while the remaining parameters and functions of y may be chosen freely.

Similarly, after substituting the parameters obtained in Eq (4.5) into the quadratic ansatz Eq (4.4), direct substitution into the bilinear equation (2.22) gives an identically vanishing residual. Therefore, the resulting lump solution is verified in the bilinear form and, through the transformation Eq (2.20), satisfies the original equation Eq (2.12). Figure 6 illustrates lump waves, which are localized rational solutions of Eq (2.12) characterized by a single non-dispersive peak that decays algebraically in all spatial directions. Unlike solitons, lump waves typically remain localized while preserving their overall structure. In Figure 6(a), where the coefficients are constant, the solution exhibits the classical symmetric lump profile with isotropic decay. In Figure 6(b), the periodic coefficient introduces oscillatory background modulation around the lump, while the central profile remains well-localized. In Figure 6(c), the hyperbolic coefficient $\tanh\left(\frac{y}{5}\right)$ generates a gradual spatial variation, resulting in an asymmetric stretching and tilting of the lump profile. In Figure 6(d), the coefficient $3\sin(e^y)$ produces a stronger periodic modulation, giving rise to a more structured background and a pronounced deformation of the localized wave. These observations demonstrate that the variable coefficients primarily control the geometry and background modulation of the lump rather than its existence. In particular, periodic profiles of $\mathcal{K}_3(y)$ and $\mathcal{K}_5(y)$ enhance the oscillatory modulation surrounding the lump, whereas gradually varying profiles modify its symmetry and orientation through changes in the local phase and effective dispersion. Consequently, within the analytical solution family and plotted parameter ranges, the variable coefficients modify the geometry, orientation, and background modulation of the localized rational-wave profiles.

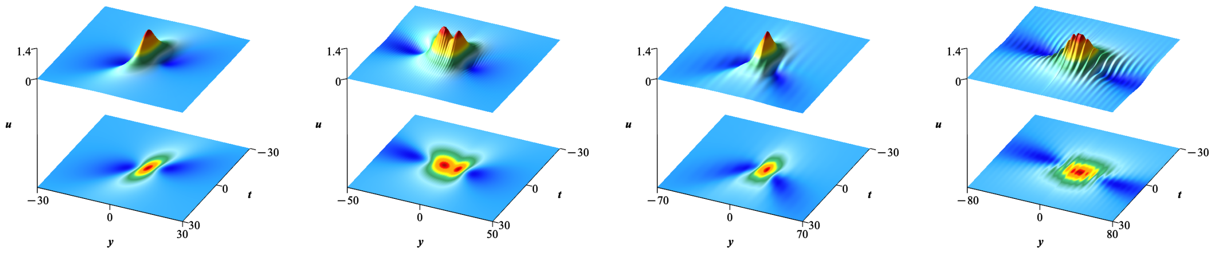

(a) **(b)** **(c)** **(d)**

Figure 6. Evolution of the lump wave Eq (4.4). The plots show the corresponding solution $u(x, y, t)$ with $x = 0$. The common parameters are $a_1 = 1, a_3 = -\frac{2}{3}, a_4 = 1, a_5 = 1, a_7 = \frac{1}{2}, a_8 = 1, C_1 = 1, C_2 = -1$. The parameters used for each panel are: **(a)** $\mathcal{K}_3(y) = -1, \mathcal{K}_4(y) = 2, \mathcal{K}_5(y) = 1$, **(b)** $\mathcal{K}_3(y) = \sin(4y), \mathcal{K}_4(y) = 3, \mathcal{K}_5(y) = \tanh\left(\frac{y}{2}\right)$, **(c)** $\mathcal{K}_3(y) = \tanh\left(\frac{y}{5}\right), \mathcal{K}_4(y) = 3, \mathcal{K}_5(y) = \sin^2\left(\frac{y}{3}\right)$, and **(d)** $\mathcal{K}_3(y) = 3\sin(e^y), \mathcal{K}_4(y) = 3, \mathcal{K}_5(y) = \cos(y)$.

4.3. Interaction between a lump and two soliton waves

To derive the mixed solution $u = \frac{6}{C_1}(\ln\xi)_{xx}$ which describes the interaction between one lump and two soliton waves, we define the auxiliary function ξ as a combination of quadratic and exponential functions.

$$\xi = (a_1x + a_2\omega_1(y) + a_3t + a_4)^2 + (a_5x + a_6\omega_2(y) + a_7t + a_8)^2 + \lambda_1 e^{-\rho\theta_1} + \lambda_2 e^{\rho\theta_1} + a_9, \tag{4.6}$$

where $\theta_1 = a_{10}x + a_{11}\omega_3(y) + a_{12}t + a_{13}$. The parameters a_i, $i = 1, \ldots, 13$ and λ_1, λ_2, and ρ are unknown and must be identified. Similar to the previous steps, by substituting this function into Eq (2.22) and solving the resulting equation, we can derive the relationships between the unknowns as follows:

$$\begin{aligned}
&\omega_1(y) = -\frac{1}{a_1a_2}\int \frac{C_2(a_3^2 - a_7^2) + a_1^2\mathcal{K}_5(y) + a_1a_3\mathcal{K}_3(y)}{\mathcal{K}_4(y)}dy, \quad \omega_2(y) = -\frac{a_7}{a_1a_6}\int \frac{2a_3C_2 + a_1\mathcal{K}_3(y)}{\mathcal{K}_4(y)}dy,\\
&\omega_3(y) = -\frac{a_{10}}{3a_1^2a_{11}}\int \frac{3a_3^2C_2 - a_7^2C_2 + 3a_1a_3\mathcal{K}_3(y) + 3a_1^2\mathcal{K}_5(y)}{\mathcal{K}_4(y)}dy, \quad \rho = \frac{a_7\sqrt{-3C_2}}{3a_{10}a_1},\\
&a_5 = 0, \quad a_{12} = \frac{a_3a_{10}}{a_1}, \quad \lambda_1 = -\frac{3a_1^4(C_2a_7^2a_9 + 3a_1^4)}{C_2^2a_7^4\lambda_2}.
\end{aligned} \tag{4.7}$$

For the obtained hybrid solution to be a regular real solution, it is necessary that $\xi > 0$ throughout the considered domain. Since ξ is the sum of two squares, two positive exponential terms, and the constant a_9, we require $\lambda_1, \lambda_2, a_9 > 0$. From Eq (4.7), this implies $C_2 < 0$ and $a_9 > \frac{3a_1^4}{-C_2a_7^2}$. Therefore, a_1, a_2, a_6, a_7, a_{10}, C_2, and $\mathcal{K}_4(y)$ are nonzero, while the remaining parameters and functions of y may be chosen freely. Similarly, after substituting the parameters obtained in Eq (4.7) into the ansatz Eq (4.6), the corresponding test function is obtained. Applying the transformation Eq (2.20) then yields a hybrid solution consisting of two soliton waves and one lump wave. Substitution of the resulting auxiliary function into the bilinear equation confirms that the corresponding residual vanishes identically. Therefore, through the transformation Eq (2.20), the obtained hybrid solution satisfies Eq (2.12).

Figure 7 illustrates hybrid profiles containing lump and exponential-wave components under different parameter and coefficient choices. Figure 7(a) shows a localized lump together with approximately symmetric V-shaped structures. Figure 7(b) presents more tilted components and a slightly stretched localized peak. Figure 7(c) exhibits a localized structure embedded in a periodically modulated background, while Figure 7(d) displays a strongly deformed cross-like configuration. These profiles illustrate coefficient-dependent changes in geometry, orientation, and background modulation. They do not, by themselves, establish energy exchange, dynamical stability, bound-state formation, or interaction strength.

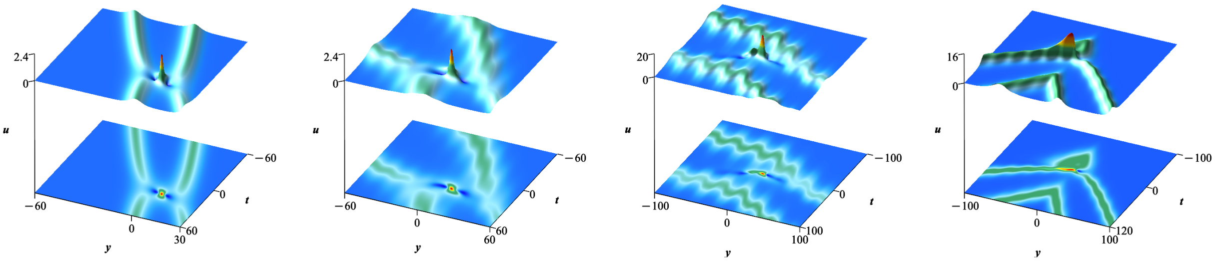

(a) (b) (c) (d)

Figure 7. Evolution of the interaction between one lump and two soliton waves described by the hybrid solution Eq (4.6). The plots show the corresponding solution $u(x, y, t)$ with $x = 0$. The common parameters are $a_1 = \frac{1}{2}$, $a_3 = \frac{1}{8}$, $a_4 = 0$, $a_6 = 1$, $a_7 = \frac{1}{2}$, $a_8 = 0$, $a_9 = 1$, $a_{10} = 6$, $a_{13} = 0$, $\lambda_2 = \frac{1}{5}$, $C_2 = -1$. For the individual panels, the parameters are: **(a)** $C_1 = 1$, $\mathcal{K}_3(y) = 1$, $\mathcal{K}_4(y) = 2$, $\mathcal{K}_5(y) = 1$, **(b)** $C_1 = \frac{1}{2}$, $\mathcal{K}_3(y) = \tanh\left(\frac{y}{5}\right)$, $\mathcal{K}_4(y) = 3$, $\mathcal{K}_5(y) = \sin^2\left(\frac{y}{5}\right)$, **(c)** $C_1 = \frac{1}{8}$, $\mathcal{K}_3(y) = \tanh\left(\frac{y}{5}\right)$, $\mathcal{K}_4(y) = 3$, $\mathcal{K}_5(y) = \sin^3\left(\frac{y}{5}\right)$, and **(d)** $C_1 = \frac{1}{8}$, $\mathcal{K}_3(y) = \sin\left(\frac{y}{3}\right)$, $\mathcal{K}_4(y) = 3$, $\mathcal{K}_5(y) = \tanh\left(\frac{y}{5}\right)$.

Overall, the graphical results presented in Figures 1–7 consistently demonstrate that the variable coefficients $\mathcal{K}_3(y)$, $\mathcal{K}_4(y)$, and $\mathcal{K}_5(y)$ provide a mechanism for modifying the displayed wave profiles in the proposed variable-coefficient model. Although these coefficients do not alter the integrability conditions established in this work, they significantly influence the geometry and propagation of the resulting localized waves through the phase functions appearing in the Hirota formulation. In particular, the coefficient $\mathcal{K}_3(y)$, associated with the mixed space-time derivative, primarily affects the propagation direction, wave inclination, and interaction behavior. The coefficient $\mathcal{K}_4(y)$, multiplying the mixed spatial derivative, governs the accumulation of the transverse phase and consequently controls the spatial orientation, bending, and rotation of the wave profiles. Meanwhile, the coefficient $\mathcal{K}_5(y)$, which modifies the longitudinal dispersive contribution, influences the effective dispersion of the system, leading to changes in wave width, localization, and modulation. These effects are consistently observed in the one-, two-, three-, and four-soliton solutions, as well as in the breather, lump, and hybrid lump–soliton solutions. Therefore, within the analytical solution families and parameter ranges considered here, the variable coefficients provide a mechanism for modifying propagation, geometry, and interaction patterns while preserving localization under the derived coefficient conditions.

5. Conclusions

In this work, we investigated a (2+1)-dimensional variable-coefficient nonlinear evolution equation. The Painlevé analysis identified several compatibility branches, and we focused on the Set 4 branch, in which $\mathcal{K}_1(y) = C_1$ and $\mathcal{K}_2(y) = C_2$, while $\mathcal{K}_3(y)$, $\mathcal{K}_4(y)$, and $\mathcal{K}_5(y)$ remain variable. Under these conditions, we explicitly derived and verified one-, two-, three-, and four-soliton solutions. The three-soliton pairwise factorization property $\mathcal{A}_{123} = \mathcal{A}_{12}\mathcal{A}_{13}\mathcal{A}_{23}$, together with the verified four-soliton case, motivates the proposed general N-soliton expression in Eq (3.15). However, a complete proof for arbitrary N remains an open problem.

The present framework also has some mathematical limitations. In particular, the Painlevé test provides a strong necessary indication of integrability but does not by itself establish a complete integrable structure, such as a Lax pair. Similarly, the explicitly verified multi-soliton solutions and the proposed general N-soliton form provide constructive evidence but do not fully characterize all possible integrable properties of the equation. Therefore, important future directions are to investigate whether a Lax pair, conservation laws, and Darboux transformations can be constructed while preserving the special structure identified here: only $\mathcal{K}_1(y)$ and $\mathcal{K}_2(y)$ are required to be constant, whereas $\mathcal{K}_3(y)$, $\mathcal{K}_4(y)$, and $\mathcal{K}_5(y)$ remain variable. This special constant/variable coefficient balance may impose additional restrictions on the deeper integrable structure of the equation. Higher-order rogue-wave and rational solutions are also worth studying under the same coefficient condition. These problems may provide a clearer understanding of the unique integrability features of variable-coefficient systems.

Author contributions

Majid Madadi: Software, visualization, methodology, validation, conceptualization, writing–original draft; Yakup Yildirim: Software, visualization, methodology, conceptualization, writing–original draft; Lanre Akinyemi: Software, validation, methodology, conceptualization, writing–original draft; Solomon Manukure: Methodology, visualization, validation, writing–original draft. All authors have read and approved the final version of the manuscript for publication.

Use of Generative-AI tools declaration

The authors declare they have not used Artificial Intelligence (AI) tools in the creation of this article.

Conflict of interest

All authors declare no conflicts of interest in this paper.

References

1. S. Sáez, On the modified generalized multidimensional KP equation in plasma physics and fluid dynamics in (3 + 1) dimensions, *J. Math. Chem.*, **61** (2023), 125–143. http://doi.org/10.1007/s10910-022-01412-0

2. B. Liu, Q. Zhao, X. Li, Step-like initial value problem and Whitham modulation in fluid dynamics to a generalized derivative nonlinear Schrödinger equation, *Phys. Fluids*, **36** (2024), 066109. http://doi.org/10.1063/5.0210864

3. R. Ali, Z. Zhang, H. Ahmad, Exploring soliton solutions in nonlinear spatiotemporal fractional quantum mechanics equations: An analytical study, *Opt. Quant. Electron.*, **56** (2024), 838. http://doi.org/10.1007/s11082-024-06370-2

4. B. Q. Li, Y. L. Ma, Optical soliton resonances and soliton molecules for the Lakshmanan–Porsezian–Daniel system in nonlinear optics, *Nonlinear Dyn.*, **111** (2023), 6689–6699. http://doi.org/10.1007/s11071-022-08195-8

5. L. Akinyemi, Robustness of localized waves under temporal modulation in higher-dimensional nonlinear evolution equations, *Phys. Lett. A*, **576** (2026), 131411. http://doi.org/10.1016/j.physleta.2026.131411

6. M. Madadi, L. Akinyemi, K. Hosseini, Wronskian and rational solutions of a (2 + 1)-dimensional nonlinear evolution equation with time-dependent coefficients, *Nonlinear Dyn.*, **114** (2026), 274. http://doi.org/10.1007/s11071-025-12151-7

7. J. L. Ji, Z. N. Zhu, On a nonlocal modified Korteweg–de Vries equation: Integrability, Darboux transformation and soliton solutions, *Commun. Nonlinear Sci.*, **42** (2017), 699–708. http://doi.org/10.1016/j.cnsns.2016.06.015

8. K. Hosseini, M. Samavat, M. Mirzazadeh, S. Salahshour, D. Baleanu, A new (4 + 1)-dimensional Burgers equation: Its Bäcklund transformation and real and complex N-kink solitons, *Int. J. Appl. Comput. Math.*, **8** (2022), 172. http://doi.org/10.1007/s40819-022-01359-5

9. S. M. Grudsky, V. V. Kravchenko, S. M. Torba, Realization of the inverse scattering transform method for the Korteweg–de Vries equation, *Math. Method. Appl. Sci.*, **46** (2023), 9217–9251. http://doi.org/10.1002/mma.9049

10. M. A. Akbar, L. Akinyemi, S. W. Yao, A. Jhangeer, H. Rezazadeh, M. M. A. Khater, et al., Soliton solutions to the Boussinesq equation through sine-Gordon method and Kudryashov method, *Results Phys.*, **25** (2021), 104228. http://doi.org/10.1016/j.rinp.2021.104228

11. A. H. Arnous, K. Hosseini, M. A. S. Murad, S. Kumar, Soliton structures, modulational instability, and chaotic dynamics of the coupled Schrödinger–Boussinesq equation, *Chaos Soliton. Fract.*, **206** (2026), 117969. http://doi.org/10.1016/j.chaos.2026.117969

12. A. Farooq, H. W. A. Riaz, S. Rehman, M. M. Mamun, W. X. Ma, Analytical and numerical soliton solutions of the Shynaray II-A equation using the $\left(\frac{G'}{G}, \frac{1}{G}\right)$-expansion method and regularization-based neural networks, *Math. Method. Appl. Sci.*, **49** (2026), 9814–9831. http://doi.org/10.1002/mma.70566

13. K. Zhang, Z. Ge, J. Cao, Novel insights into the truncated M-fractional Shynaray-IIA equation: New wave solutions and its dynamic behavior, *Netw. Heterog. Media*, **21** (2026), 1197–1226. http://doi.org/10.3934/nhm.2026048

14. M. Z. Raza, M. A. B. Iqbal, A. Khan, D. K. Almutairi, T. Abdeljawad, Soliton solutions of the (2 + 1)-dimensional Jaulent–Miodek evolution equation via effective analytical techniques, *Sci. Rep.*, **15** (2025), 3495. http://doi.org/10.1038/s41598-025-87785-z

15. W. X. Qiu, Z. Z. Si, D. S. Mou, C. Q. Dai, J. T. Li, W. Liu, Data-driven vector degenerate and nondegenerate solitons of coupled nonlocal nonlinear Schrödinger equation via improved PINN algorithm, *Nonlinear Dyn.*, **113** (2025), 4063–4076. http://doi.org/10.1007/s11071-024-09648-y

16. Z. Li, M. Wu, E. Hussain, Y. Yildirim, Exactly explicit solutions of a (2 + 1)-dimensional conformable fractional diffusive predator–prey model via neural networks method, *Front. Phys.*, **14** (2026), 1824530. http://doi.org/10.3389/fphy.2026.1824530

17. W. X. Qiu, K. L. Geng, B. W. Zhu, W. Liu, J. T. Li, C. Q. Dai, Data-driven forward-inverse problems of the 2-coupled mixed derivative nonlinear Schrödinger equation using deep learning, *Nonlinear Dyn.*, **112** (2024), 10215–10228. http://doi.org/10.1007/s11071-024-09605-9

18. Z. Li, E. Hussain, Bifurcation analysis and chaotic behaviors of a traveling-wave solution to the Zhiber–Shabat equation with a truncated M-fractional derivative, *Fractal Fract.*, **10** (2026), 335. http://doi.org/10.3390/fractalfract10050335

19. Z. Yang, W. P. Zhong, M. Belić, Dark localized waves in shallow waters: Analysis within an extended Boussinesq system, *Chinese Phys. Lett.*, **41** (2024), 044201. http://doi.org/10.1088/0256-307X/41/4/044201

20. W. P. Zhong, Z. Yang, M. Belić, W. Zhong, Breather solutions of the nonlocal nonlinear self-focusing Schrödinger equation, *Phys. Lett. A*, **395** (2021), 127228. http://doi.org/10.1016/j.physleta.2021.127228

21. M. Madadi, M. Inc, Determinantal solutions to the (3 + 1)-dimensional Painlevé-type evolution equation: Higher-order rogue and soliton waves, *Wave Motion*, **139** (2025), 103624. http://doi.org/10.1016/j.wavemoti.2025.103624

22. J. Ahmad, S. Akram, K. Noor, M. Nadeem, A. Bucur, Y. Alsayaad, Soliton solutions of fractional extended nonlinear Schrödinger equation arising in plasma physics and nonlinear optical fiber, *Sci. Rep.*, **13** (2023), 10877. http://doi.org/10.1038/s41598-023-37757-y

23. A. Warn-Varnas, S. A. Chin-Bing, D. B. King, J. Hawkins, K. Lamb, Effects on acoustics caused by ocean solitons, Part A: Oceanography, *Nonlinear Anal. Theor.*, **71** (2009), e1807–e1817. http://doi.org/10.1016/j.na.2009.02.104

24. W. A. Faridi, M. Iqbal, M. B. Riaz, S. A. AlQahtani, A. M. Wazwaz, The fractional soliton solutions of a dynamical system arising in plasma physics: The comparative analysis, *Alex. Eng. J.*, **95** (2024), 247–261. http://doi.org/10.1016/j.aej.2024.03.061

25. S. Singh, K. Sakkaravarthi, K. Murugesan, R. Sakthivel, Benjamin–Ono equation: Rogue waves, generalized breathers, soliton bending, fission, and fusion, *Eur. Phys. J. Plus*, **135** (2020), 823. http://doi.org/10.1140/epjp/s13360-020-00808-8

26. U. Younas, T. A. Sulaiman, J. Ren, A. Yusuf, Lump interaction phenomena to the nonlinear ill-posed Boussinesq dynamical wave equation, *J. Geom. Phys.*, **178** (2022), 104586. http://doi.org/10.1016/j.geomphys.2022.104586

27. M. A. Ablowitz, P. A. Clarkson, *Solitons, nonlinear evolution equations and inverse scattering*, Cambridge: Cambridge University Press, 1991. http://doi.org/10.1017/CBO9780511623998

28. J. Weiss, M. Tabor, G. Carnevale, The Painlevé property for partial differential equations, *J. Math. Phys.*, **24** (1983), 522–526. http://doi.org/10.1063/1.525721

29. M. Jimbo, M. D. Kruskal, T. Miwa, Painlevé test for the self-dual Yang–Mills equation, *Phys. Lett. A*, **92** (1982), 59–60. http://doi.org/10.1016/0375-9601(82)90291-2
30. W. P. Zhong, M. Belić, G. Assanto, B. A. Malomed, T. Huang, Light bullets in the spatiotemporal nonlinear Schrödinger equation with a variable negative diffraction coefficient, *Phys. Rev. A*, **84** (2011), 043801. http://doi.org/10.1103/PhysRevA.84.043801
31. H. W. A. Riaz, A. Farooq, A (2 + 1) modified KdV equation with time-dependent coefficients: Exploring soliton solution via Darboux transformation and artificial neural network approach, *Nonlinear Dyn.*, **113** (2025), 3695–3711. http://doi.org/10.1007/s11071-024-10423-2
32. H. W. A. Riaz, A. Farooq, Exact solutions and nonlinear wave interactions in a non-commutative coupled dispersionless system with variable coefficients, *Nonlinear Dyn.*, **113** (2025), 35125–35139. http://doi.org/10.1007/s11071-025-11833-6
33. X. Yin, D. Zuo, Soliton, lump and hybrid solutions of a generalized (2+1)-dimensional Benjamin–Ono equation in fluids, *Nonlinear Dyn.*, **113** (2025), 8839–8857. http://doi.org/10.1007/s11071-024-10552-8
34. M. J. Ablowitz, H. Segur, On the evolution of packets of water waves, *J. Fluid Mech.*, **92** (1979), 691–715. http://doi.org/10.1017/S0022112079000835
35. D. E. Pelinovsky, Y. A. Stepanyants, Y. S. Kivshar, Self-focusing of plane dark solitons in nonlinear defocusing media, *Phys. Rev. E*, **51** (1995), 5016–5026. http://doi.org/10.1103/PhysRevE.51.5016
36. Y. Y. Li, H. C. Hu, Nonlocal symmetries and interaction solutions of the Benjamin–Ono equation, *Appl. Math. Lett.*, **75** (2018), 18–23. http://doi.org/10.1016/j.aml.2017.06.012
37. N. Taghizadeh, M. Mirzazadeh, F. Farahrooz, Exact soliton solutions for the second-order Benjamin–Ono equation, *Appl. Appl. Math.*, **6** (2011), 2125–2136.
38. Y. S. Özkan, Double reduction of the second-order Benjamin–Ono equation via conservation laws and the exact solutions, *Balıkesir Üniversitesi Fen Bilimleri Enstitüsü Dergisi*, **23** (2021), 210–223. http://doi.org/10.25092/baunfbed.848234
39. G. He, L. He, The application of trigonal curve theory to the second-order Benjamin–Ono hierarchy, *Adv. Differ. Equ.*, **2014** (2014), 195. http://doi.org/10.1186/1687-1847-2014-195
40. W. Liu, High-order rogue waves of the Benjamin–Ono equation and the nonlocal nonlinear Schrödinger equation, *Mod. Phys. Lett. B*, **31** (2017), 1750269. http://doi.org/10.1142/S0217984917502694
41. L. Akinyemi, Shallow ocean soliton and localized waves in extended (2 + 1)-dimensional nonlinear evolution equations, *Phys. Lett. A*, **463** (2023), 128668. http://doi.org/10.1016/j.physleta.2023.128668
42. J. Boussinesq, Théorie de l'intumescence liquide appelée onde solitaire ou de translation se propageant dans un canal rectangulaire, *Les Comptes Rendus de l'Académie des Sciences*, **72** (1871), 755–759.
43. M. J. Ablowitz, R. Haberman, Resonantly coupled nonlinear evolution equations, *J. Math. Phys.*, **16** (1975), 2301–2305. http://doi.org/10.1063/1.522460
44. V.E. Zakharov, On stochastization of one-dimensional chains of nonlinear oscillations, *Sov. Phys. JETP*, **38** (1974), 108–110.

45. M. Toda, Studies of a non-linear lattice, *Phys. Rep.*, **18** (1975), 1–123. http://doi.org/10.1016/0370-1573(75)90018-6

46. S. H. Liu, B. Tian, M. Wang, Painlevé analysis, bilinear form, Bäcklund transformation, solitons, periodic waves and asymptotic properties for a generalized Calogero–Bogoyavlenskii–Konopelchenko–Schiff system in a fluid or plasma, *Eur. Phys. J. Plus*, **136** (2021), 917. http://doi.org/10.1140/epjp/s13360-021-01828-8

47. R. Hirota, *The direct method in soliton theory*, Cambridge: Cambridge University Press, 2004. http://doi.org/10.1017/CBO9780511543043

48. C. Gilson, F. Lambert, J. Nimmo, R. Willox, On the combinatorics of the Hirota D-operators, *Proc. R. Soc. A*, **452** (1996), 223–234. http://doi.org/10.1098/rspa.1996.0013

49. A. R. Osborne, Nonlinear ocean waves and the inverse scattering transform, In: *Scattering: Scattering and inverse scattering in pure and applied science*, 2002, 637–666. https://doi.org/10.1016/B978-012613760-6/50033-49

50. X. H. Wu, Y. T. Gao, X. Yu, L. Q. Li, C. C. Ding, Vector breathers, rogue and breather-rogue waves for a coupled mixed derivative nonlinear Schrödinger system in an optical fiber, *Nonlinear Dyn.*, **111** (2023), 5641–5653. http://doi.org/10.1007/s11071-022-08058-2

51. N. Gupta, A. K. Alex, R. Johari, S. Choudhry, S. Kumar, A. Ahmad, et al., Formation of elliptical q-Gaussian breather solitons in diffraction-managed nonlinear optical media: Effect of cubic–quintic nonlinearity, *J. Opt.*, **53** (2024), 4037–4049. http://doi.org/10.1007/s12596-023-01349-w